This article was downloaded by: *[Oak Ridge National Laboratory]*
On: *28 May 2009*
Access details: *Access Details: [subscription number 909492212]*
Publisher *Taylor & Francis*
Informa Ltd Registered in England and Wales Registered Number: 1072954 Registered office: Mortimer House, 37-41 Mortimer Street, London W1T 3JH, UK

Dekker Encyclopedia of Nanoscience and Nanotechnology, Second Edition
Publication details, including instructions for authors and subscription information:
http://www.informaworld.com/smpp/title~content=t908795069

Aberration-Corrected Z-Contrast STEM: Semiconducting Nanocrystals

James R. McBride [a]; Andrew R. Lupini [b]; Stephen J. Pennycook [b]; Sandra J. Rosenthal [c]
[a] Department of Chemistry, Vanderbilt University, Nashville, Tennessee, U.S.A. [b] Materials Science and Technology Division, Oak Ridge National Laboratory, Oak Ridge, Tennessee, U.S.A. [c] Department of Chemistry and Physics, Vanderbilt University, Nashville, Tennessee, U.S.A.

Online Publication Date: 25 March 2009

To cite this Section McBride, James R., Lupini, Andrew R., Pennycook, Stephen J. and Rosenthal, Sandra J.(2009)'Aberration-Corrected Z-Contrast STEM: Semiconducting Nanocrystals',Dekker Encyclopedia of Nanoscience and Nanotechnology, Second Edition,1:1,1 — 21

PLEASE SCROLL DOWN FOR ARTICLE

Full terms and conditions of use: http://www.informaworld.com/terms-and-conditions-of-access.pdf

This article may be used for research, teaching and private study purposes. Any substantial or systematic reproduction, re-distribution, re-selling, loan or sub-licensing, systematic supply or distribution in any form to anyone is expressly forbidden.

The publisher does not give any warranty express or implied or make any representation that the contents will be complete or accurate or up to date. The accuracy of any instructions, formulae and drug doses should be independently verified with primary sources. The publisher shall not be liable for any loss, actions, claims, proceedings, demand or costs or damages whatsoever or howsoever caused arising directly or indirectly in connection with or arising out of the use of this material.

Aberration-Corrected Z-Contrast STEM: Semiconducting Nanocrystals

James R. McBride
Department of Chemistry, Vanderbilt University, Nashville, Tennessee, U.S.A.

Andrew R. Lupini
Stephen J. Pennycook
Materials Science and Technology Division, Oak Ridge National Laboratory, Oak Ridge, Tennessee, U.S.A.

Sandra J. Rosenthal
Department of Chemistry and Physics, Vanderbilt University, Nashville, Tennessee, U.S.A.

Abstract
The development of aberration-corrected scanning transmission electron microscopy (STEM) has provided new insight in the development of nanomaterials. Specifically, atomic number contrast STEM, or Z-STEM, has been applied to elucidate the structure of cadmium-based semiconductor nanocrystals. With sub-angstrom detail, the images obtained elucidated the effects of surfactants on the nanocrystal shape, showed the precise coverage of epitaxial shells for core/shell quantum dots, as well as provided the first images of the atomic structure of alloy nanocrystals.

Downloaded By: [Oak Ridge National Laboratory] At: 19:18 28 May 2009

Semiconducting nanocrystals are one of the most beautiful examples of how new and fascinating physical properties arise in the nano-regime. As first demonstrated by Louis Brus, the band gap, and in essence, the color of a semiconductor becomes size-dependent when the diameter is reduced to below the bulk Bohr exciton diameter.[1] This allows for precise tuning of the absorption and emission properties by simply controlling the nanocrystal's diameter. In 1993, Murray, Norris, and Bawendi published the synthesis that would form the basis of the production of monodisperse, colloidal nanocrystals.[2] This has become the foundation of the nanocrystal field, which has since grown to not only include fundamental investigations into the properties of the nanocrystals themselves, but also the development of practical applications. Efforts are currently focused on the use of colloidal nanocrystals or ''quantum dots'' for the development of fluorescent probes for biological imaging, phosphors for solid-state lighting, and light harvesters for photovoltaics.[3–10] Although great strides have been made towards the development of these applications, much more basic research is needed to develop them into powerful, reliable, and competitive technologies.

One of the most useful properties of nanocrystals is their large surface-to-volume ratio. For example, in a 1.2 nm diameter nanocrystal, nearly all of the atoms are surface atoms. This results in the surface dominating the chemical and physical properties of the nanocrystal. The surface consists of a mixture of unpassivated atoms with dangling bonds and atoms that are passivated with surfactants. The electronic, optical, and physical properties of the nanocrystal are extremely sensitive to the surface conditions. Dangling bonds can act as charge traps, reducing the emission efficiency. They are also able to easily take part in chemical reactions. For example, oxygen can bind to the unpassivated atoms forming an oxide, which can cause photo-brightening and eventually quenching.[11] The presence and type of passivating ligand can also be chosen to tailor the properties of the nanocrystal in controlled ways, such as improving the emission efficiency, or quenching the emission completely, if desired. The surface can also be affected by ''shelling''; core/shell quantum dots have an outer coating of a wide bandgap semiconductor to passivate the surface and confine electrons and holes to the core. The thickness and total coverage of the shell dictates the quantum yield and resistance to photobleaching of core/shell quantum dots.

The importance of the surface structure has driven the application of aberration-corrected, atomic number contrast scanning transmission electron microscopy (Z-STEM) to characterize nanocrystals. This technique allows for direct imaging the nanocrystal's core and surface structure with sub-angstrom resolution. Additionally, the image intensity is dependent on chemical composition and thickness affording an unparallel view of the nanocrystal. This entry will review our recent work in utilizing this technique to study colloidal cadmium-based semiconductor nanocrystals. Specifically, Z-STEM was used for (1) observing the effect of surfactant on the nanocrystal shape; (2) guiding the development of near unity quantum

Dekker Encyclopedia of Nanoscience and Nanotechnology, Second Edition DOI: 10.1081/E-ENN2-120044858
Copyright © 2009 by Taylor & Francis. All rights reserved.

Downloaded By: [Oak Ridge National Laboratory] At: 19:18 28 May 2009

yield core/shell nanocrystals; and (3) the characterization of homogeneous nanocrystal alloys. These applications rely on the unique capability of Z-STEM to simultaneously provide sub-angstrom resolution, allowing individual atoms to be imaged, and chemical identification of the elements present.

SYNTHESIS OF CdSe NANOCRYSTALS

The current methods for synthesizing CdSe nanocrystals follow procedures similar to those of Bowen-Katari, Colvin, and Alivisatos, which eliminated the need for size-selective precipitation to produce monodisperse samples.[12] In this preparation, 99% trioctylphosphine oxide (TOPO) and tri-*n*-butylphosphine (TBP) is used as received from Aldrich. Se (60 mesh powder) is dissolved in TBP and followed by the addition of dimethylcadmium. The injection solution of cadmium and selenium in TBP is then diluted 4 : 1 with TBP and injected into the reaction vessel of TOPO at ~350°C. The solution is removed from heat and allowed to cool under argon, which prevents oxidation of the nanocrystal surface. To recover nanocrystals from the solid, room temperature TOPO mixture, methanol is added to dissolve the TOPO and precipitate the nanocrystals, which are then recovered by filtration. To make nanocrystals with an absorption maximum larger than 580 nm, the reaction is cooled from 350°C to 320°C and the nanocrystals are allowed to grow while the size is monitored by drawing aliquots from solution and monitoring the absorption spectra. Using this growth method, the initial tight size distribution is lost. This can be overcome by the addition of additional reagent solution to "focus" the size distribution.

The use of dimethylcadmium to produce high-quality nanocrystals is still common. However, Peng and Peng demonstrated the use of CdO as a benign source of cadmium.[13] In this one-pot approach, CdO, TOPO and either hexylphosphonic acid (HPA) or tetradecylphosphonic acid (TDPA) are loaded into a three-neck flask. At temperatures above 270°C, the phosphonic acid complexes with the CdO forming a clear and colorless solution. After the formation of the colorless cadmium phosphonate complex, Se : TBP is injected into the reaction, which initiates the formation of nanocrystals. This method can also be used to produce high-quality CdS and CdTe nanocrystals by replacement of the anion solvated by TBP.[14]

Weller and co-workers developed a similar synthetic methodology using cadmium acetate $Cd(CH_3CO_2)_2$ as the precursor.[15] In this method, a stock selenium solution of trioctylphosphine:Se (TOP : Se) is added to a mixture of TOPO : hexadecylamine (HDA) : TDPA at 120°C. This is then heated to 300°C to which a stock solution of cadmium acetate and selenium dissolved in TOP is rapidly injected. Both the cadmium and selenium stock solutions are stored inside a glove box under nitrogen atmosphere. Additionally, efforts to reduce the use of phosphine in the chemistry has led to the development of the use of oleic acid and octadecene as the surfactants, in place of TOPO and the phosphonic acids.[16]

TEM EXPERIMENTAL

Nanocrystal sample preparation for electron microscopy is, in general, simple. The as-synthesized nanocrystal powder or liquid need to be purified to remove any excess starting materials and surfactants. It is critical to develop a methodology that removes the unbound surfactants as they will deposit with the nanocrystals onto the TEM grid, making the overall sample thicker than desired, and they may also cause contamination. Contamination is believed to be beam-induced polymerization of carbonaceous materials on the carbon support. This polymer can continue to grow until the beam can no longer penetrate the specimen. The cleaning steps typically used to remove this unwanted material depend on the surfactants used during synthesis. TOPO-coated nanocrystals need only three methanol washes, TOPO-HDA nanocrystals require an inverse precipitation step in octanol, while oleic acid-coated nanocrystals require three washes with a careful mixture of chloroform and acetone.[17] Once clean, the powdered nanocrystals should be brought into solution with an appropriate solvent. For TOPO-coated nanocrystals, toluene or hexanes work well. Ultrathin carbon on formvar TEM grids purchased from Ted Pella, Inc. (part no. 01822-F) are ideal for imaging nanocrystal samples. They have an average thickness of 30 nm and are fairly resilient to sample preparations due to the formvar support. The formvar support can be removed to minimize the film thickness and subsequently the carbon background in the TEM images. For Z-STEM, lacey carbon coated with ultrathin carbon, also from Ted Pella, is used to provide the least amount of background for imaging.

After the film is cleaned, a drop of a nanocrystal solution with an optical density of less than 0.1 is placed onto the grid. Anticapillary tweezers should prevent premature drawing up of, or wicking, of the solution. A Kimwipe™ can be used to "wick" the solvent off in a controllable fashion, leaving the nanocrystals on the carbon film. Alternatively, the solvent can be allowed to evaporate, helping the nanocrystals to array and limit nanocrystal stacking and bunching. The higher the boiling point of the solvent, the longer the nanocrystals will have to order themselves on the grid. However, leaving the solvent to dry also allows for

Downloaded By: [Oak Ridge National Laboratory] At: 19:18 28 May 2009

more of the excess surfactants to accumulate on the grid, increasing the chance for contamination under the electron beam.

Since the electron beam is focused to a point in STEM, it is more susceptible to contamination and requires extra care during sample preparation. Even samples that do not contaminate under conventional TEM conditions can be problematic in STEM. To combat this, samples on ultra-thin carbon grids can be plasma cleaned for up to 20 sec in an argon/oxygen plasma cleaner. More effectively, yet more damaging to the nanocrystals, the sample can be exposed to a high intensity light bulb, either outside the microscope, or in the air lock under vacuum. Twenty minutes of the ''light bulb'' treatment can effectively eliminate contamination and allow for sustained imaging over a single area for an extended period of time.

THE MICROSCOPES

Conventional high-resolution transmission electron microscopy (HRTEM) images were obtained using a Phillips CM20 operating at 200 kV, located at Vanderbilt University. Z-STEM images were taken using the VG HB603u 300 kV aberration-corrected STEM located at Oak Ridge National Laboratories, in collaboration with Stephen J. Pennycook. Fitted with a Nion C_s corrector, the HB603u has a record-setting 0.78 Å resolution, allowing for several pixels in an image to be devoted to a single angstrom.[18] Images are collected using a high-angle annular dark field detector (HAADF), which allows for simultaneous collection of dark field (Z-STEM) and bright field images. The dark field images are formed by the highly scattered electrons, resulting in image intensities that are dependent on sample thickness and the atomic number (Z) of the atom or atomic column being imaged. Images are collected and processed using Gatan's Digitalmicrograph software. Unless otherwise noted, images are ''smoothed'' to remove any high frequency shot noise from the images. Color has been added to emphasize that the intensity is important in image interpretation.

CONVENTIONAL HIGH-RESOLUTION TRANSMISSION ELECTRON MICROSCOPY (HRTEM) FOR CHARACTERIZATION OF NANOCRYSTALS

Conventional HRTEM is the standard technique for measuring the size, dispersity, and overall quality of a nanocrystal sample. Owing to the ability of nanocrystals to freely rotate under the electron beam, obtaining lattice resolved images of them requires quick reflexes and often a bit of luck. Unlike thin films of solids, whose crystallographic orientation is dependent on how it is sliced, nanocrystals are free to rotate on the carbon film and align themselves randomly. Fringe patterns in phase contrast imaging are used to determine the size, shape, and the crystal structure of the object being imaged. Because of the relatively small number of properly aligned nanocrystals, finding nanocrystals that are not in contact with others and facing with the zone axis towards the electron beam can be a difficult task. Using solutions with a low concentration of nanocrystals and allowing the solvent to evaporate, allowing the nanocrystals to array, is best for producing the highest number of isolated nanocrystals per area of carbon film. The difference between evaporating and ''wicking'' the nanocrystal solution can be seen in the TEM images in Fig. 1. The nanocrystals in the wicked sample, Fig. 1A, are clumped together, while those of the evaporated sample, Fig. 1B, are evenly separated into a two-dimensional array, with the distance between them dictated by sample concentration and surfactant. Highly concentrated solutions of nanocrystals form extremely dense arrays that are not useful for imaging individual nanocrystals, as shown in Fig. 1C. Fig. 2 shows the three distinct fringe patterns that can be assigned to different orientations of the nanocrystal.[19] The pattern labeled ''B'' is consistent with the [100] orientation. This is the most common orientation found, since the largest face of the nanocrystal is in contact with the carbon film. The zigzag pattern labeled ''C'' is that of the [010] orientation. To achieve this orientation, the nanocrystal must be resting on a corner

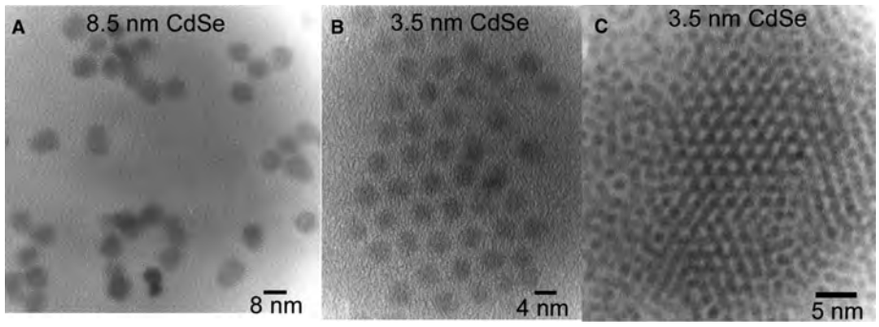

Fig. 1 TEM sample preparation. TEM images of samples that were wicked (A), not wicked (B) and overcrowded (C) are shown.

Downloaded By: [Oak Ridge National Laboratory] At: 19:18 28 May 2009

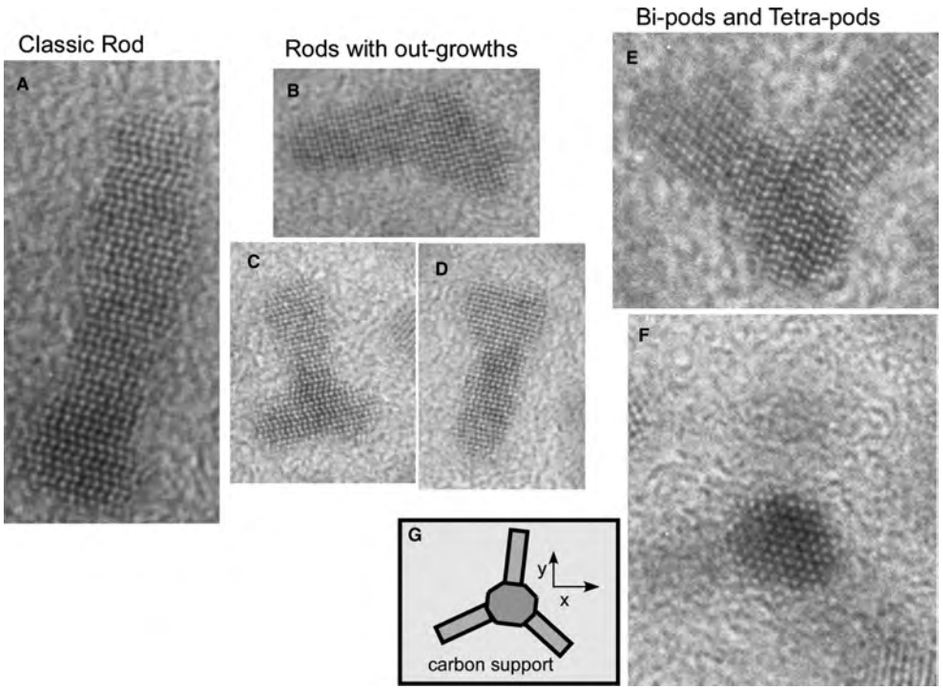

Fig. 2 Fringe patterns. (A) TEM image of randomly orientated CdSe nanocrystals. (B–D) [100], [010], [001] fringe patterns and their associated lattice spacing.

facet. The orientation labeled "D" corresponds to [001] direction and requires the nanocrystal to be sitting on end. This orientation clearly shows the hexagonal shape of wurtzite CdSe. From images like these, it is not only possible to determine the average nanocrystal size but also determine the average shape. The size of the nanocrystal can be determined either by counting the number of lattice fringes and multiplying that number times the fringe spacing or by simply determining the scale of the image and then measuring the diameter of the particle. The latter, however, requires that the microscope be precisely calibrated. Approximately 200 measurements of individual nanocrystals are needed to determine a size distribution.[19]

Large shape morphologies can be easily seen under HRTEM conditions. Fig. 3 contains HRTEM images of CdSe nanocrystal prepared under different reaction conditions. Fig. 3A is a CdSe nanorod. Fig. 3D are images of nanorods with small outgrowths, and Fig. 3E and F are TEM images of a bipod and tetrapod, respectively. The odd shapes of the nanocrystals in Fig. 3 could be the result of the large number of stacking faults [a stacking fault is a break in the regular crystal pattern,[20]] or the result of the mixture of surfactants used in the synthesis. Wurtzite CdSe nanocrystals often have zinc blende stacking faults in them due to the small energetic difference between the two phases. The nanocrystal in 3A shows several sections of zinc blende in the top half while the bottom half exhibits the normal alternating pattern of a wurtzite crystal lattice oriented in the [010] direction. From the fringes, it can be presumed that the growth is along the *c*-axis, since this is the long axis of the nanocrystal. It is also known from the CdSe nanocrystal structure that there are Cd and Se rich facets, which should create surfaces with different chemical reactivities. However, in which direction growth occurs, whether towards the Se face or the Cd face, cannot be determined. This unidirectional growth, if understood, could lead to control of facet-specific growth mechanisms such as those that formed the tetrapods in Fig. 3E and F.[14,21] Unfortunately, phase contrast imaging does not yield enough detail to differentiate the Cd- and Se-terminated facets.[11,22,23] However, Z-STEM can directly probe the chemical structure with atomic level precision. A general description of the technique is described in the following section.

ATOMIC NUMBER CONTRAST SCANNING TRANSMISSION ELECTRON MICROSCOPY (Z-STEM)

Atomic number contrast scanning transmission electron microscopy uses an atom-sized probe that scans across the sample to form an image. The electrons scattered at low angles are used to form a bright field image while those scattered at high angles are used to

Downloaded By: [Oak Ridge National Laboratory] At: 19:18 28 May 2009

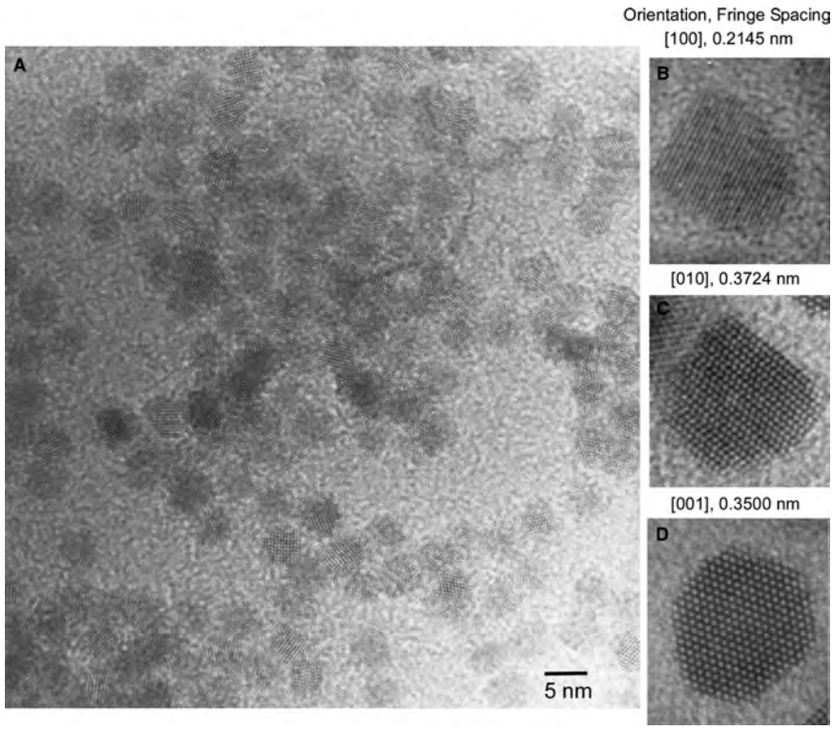

Fig. 3 TEM images of various shapes of CdSe nanocrystals. Depending on the growth conditions, nanocrystals can form shapes such as rods (A), rods with growths (B–D) and bi-pods and tetrapods (E and F). G is a cartoon illustrating the tetrapod in (F) with the fourth arm pointing in the Z direction, out of the sample plane.

form a dark field image. The bright field image is a coherent phase contrast image, similar to that formed in a comparable high-resolution TEM. High-angle scattering is generated incoherently, and leads to an incoherent image, the resolution of which is directly related to electron probe diameter. The electron probe size in STEM is limited by the beam energy, its energy spread, and by aberrations in probe-forming lenses.[24] Also, high-angle scattered electrons show a strong atomic number contrast, hence the term Z-STEM, or Z-contrast imaging, also known as HAADF imaging.[25–27] These electrons can be compared with the He ions in Rutherford Backscattering in that their energy and intensity are dependent on the material with which they interact. Electrons impinging upon a heavy atom will scatter more frequently to higher angles than those that encounter a lighter atom. Therefore, scattered electrons detected from atoms with differing atomic weights appear as intensity variations in the image, yielding elemental information directly from the image. Unlike coherent imaging techniques such as phase contrast imaging (conventional HRTEM), there are no complicated contrast changes with focus or specimen thickness.[28] This allows for direct interpretation of the images; a bright spot in the image plane corresponds directly to a scattering center in the object plane, i.e. an atom. Additionally, the intensity of the scattered electrons depends on the square of the atomic number of the scattering atom, yielding spatially resolved chemical information.[25]

As a result of the sub-angstrom probe and its imaging design, Z-STEM provides an unmatched ability to achieve structural and chemical information from individual nanostructures at the atomic level.[18,29] For example, Z-STEM tomography was recently used to determine the 3D structure of less than 10 nm Sn quantum dots embedded in Si with cubic nanometer resolution.[30] Z-STEM has been used for many years to directly image the atomic structure of grain boundaries and interfaces, even revealing specific impurity segregation sites.[31–33] A key advantage of Z-STEM is that it can be easily combined with electron energy loss spectroscopy (EELS) to achieve elemental identification with atomic resolution.[34] Today, with the successful correction of lens aberrations, Z-STEM has demonstrated 0.78 Å spatial resolution by directly imaging Si [112] atomic dumbbells.[18] The higher resolution and image contrast also results in a greatly improved sensitivity for EELS, opening many opportunities for materials science research.[35] For example, it was shown using these two techniques that rare earth dopant atoms, such as La, preferentially segregate to the amorphous crystal interfaces of Si_3N_4.[36] This level of precise information is critical for the development of nanomaterials where the placement of a single atom can drastically affect the desired properties.

A comparison between two similarly orientated CdSe nanocrystals, imaged under HRTEM and Z-STEM, is shown in Fig. 4. False color has been added to the Z-STEM image to emphasize the

Downloaded By: [Oak Ridge National Laboratory] At: 19:18 28 May 2009

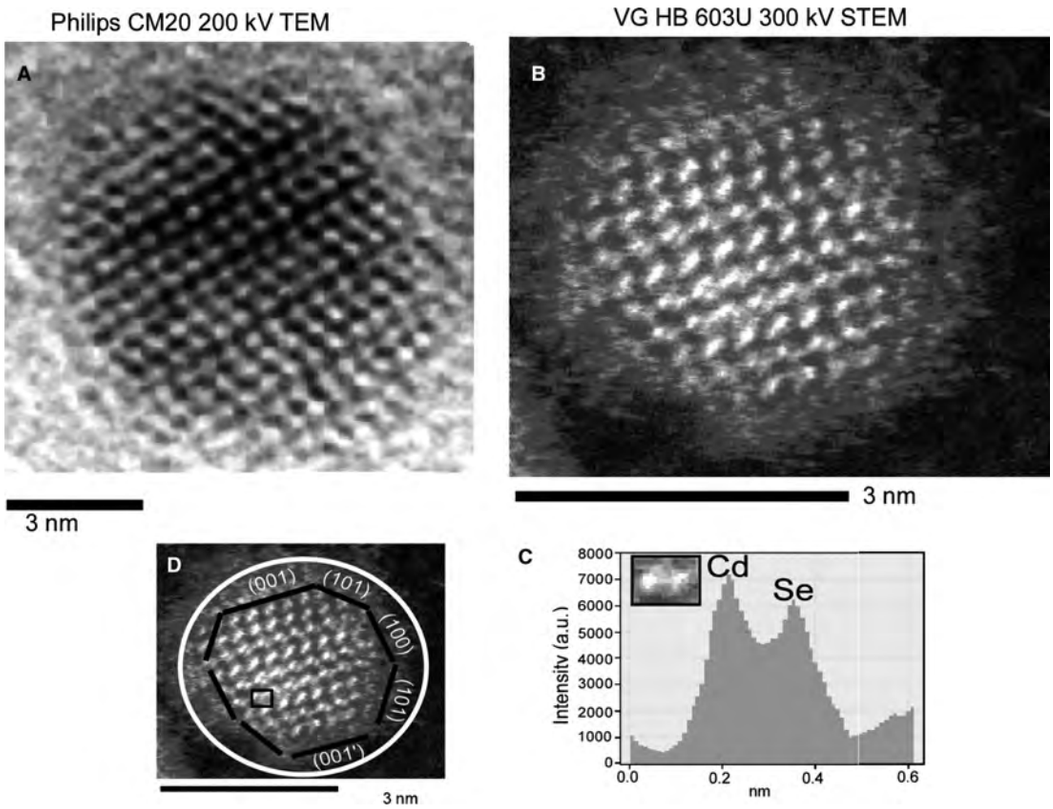

Fig. 4 TEM–Z-STEM comparison. (A) and (B) are TEM and Z-STEM images of similarly orientated CdSe nanocrystals. (C) is a line profile taken from (D) (black box) showing intensity contrast from the Cd and Se atomic columns. The intensity contrast can be used to assign specific facets in the image (D). The white circle in (D) highlights the amorphous oxide coating. *Source*: Reprinted with permission from *Nano Lett.*, **2004**, *4* (7) 1279–1283. © 2004 American Chemical Society.

importance of the image intensity. Unlike the conventional HRTEM image in Fig. 4A, chemical and structural information can be obtained directly from the intensities in the raw Z-STEM image. For example, the Cd and Se columns in Fig. 4B can be assigned from the intensity difference found in the raw image, as indicated by the intensity profile in Fig. 4C. With this information, the Cd-rich (001) and the Se-rich (001′) surfaces can be then assigned by following the alternating intensities to the surface, as shown in Fig. 4D. Additionally, since the electrons that are detected are incoherently scattered, phase contrast that produces the speckle pattern in bright field images of amorphous carbon is not present. As a result, single atoms can be imaged on the surface of an amorphous carbon film, and nanocrystal edges are clearly visible in cases where the nanocrystal is not susceptible to oxidation.[37] In the images in Fig. 4, the nanocrystal edges are oxidized owing to exposure to air, and the resultant amorphous oxide layer, which has been enclosed by a white circle, can be clearly seen in the Z-STEM image in Fig. 4D. The spots seen in the oxide are the remains of the outer surface of the nanocrystal. Individual atoms and atomic clusters can readily be found in this region; these atoms and clusters would not be visible using conventional HRTEM since there is no contrast between amorphous materials and the amorphous carbon support.

Besides the smaller probe size, an additional advantage of aberration correction is that the STEM Bright Field (BF) has about two orders of magnitude more current, enhancing the signal-to-noise resolution, making it a practically useful additional channel of information. It is obtained simultaneously with the Z-STEM image, and is equivalent to an aberration-corrected HRTEM image by the principle of reciprocity (reversing ray directions). Fig. 5 shows the simultaneous BF and Z-STEM images of a triangular shaped CdSe/CdS core/shell nanocrystal taken after the installation of the aberration corrector.[38] The BF image shows the edge of the nanocrystal more clearly, because of the reduced image delocalization, but it is still not able to detect individual atoms on the amorphous carbon support because of the lack of strong Z-contrast. The Z-STEM image does show individual atoms and small clusters on the carbon film. The

Downloaded By: [Oak Ridge National Laboratory] At: 19:18 28 May 2009

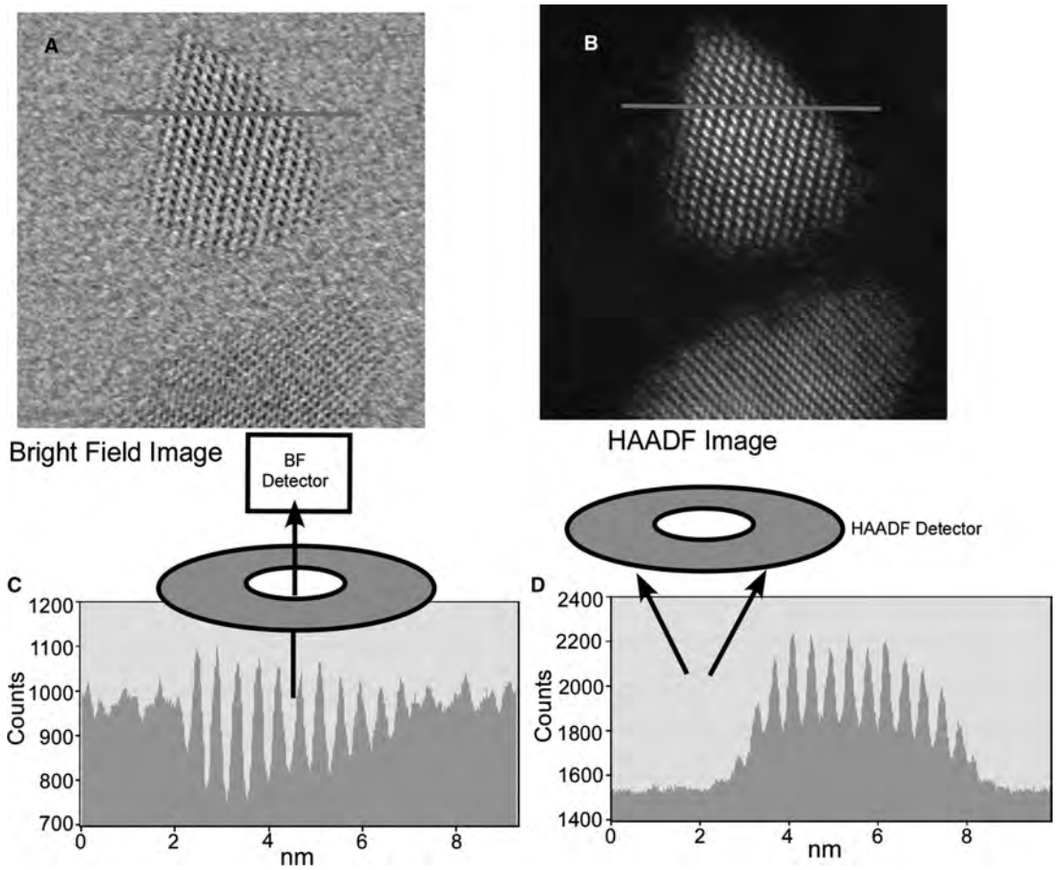

Fig. 5 Bright field vs. dark field STEM. The STEM images A (bright field) and B (dark field) are obtained simultaneously during imaging. The line profiles (C and D) show the reduction in back ground intensity afforded by dark field imaging. *Source*: Reprinted with permission from *Surf. Sci. Rep.*, **2007**, *62*, 111–157. © 2007 Elsevier B. V.

line profiles in Figs. 5C and D illustrate how the bright field image is formed by constructive and destructive interference on top of the contrast from the carbon support, whereas the Z-STEM image exhibits a sharp increase in intensity between the carbon film and the nanocrystal, indicating the precise location of the surface. However, the bright field image is still particularly useful for finding focus and for manually adjusting for astigmatism, although it should be noted that optimum focus for a bright field image is not exactly the same as optimum focus for the Z-STEM image.[28]

Z-STEM OF CdSe NANOCRYSTALS

The following figures show how easily Z-STEM images can be interpreted. There are three main orientations that allow lattice-resolved images. Examples of these are shown in Figs. 6 and 7. The images can be interpreted simply by comparison to a computer generated ''ball-and-stick'' CdSe nanocrystal model and rotating it in three dimensions to match the atomic arrangement in the Z-STEM image. This particular model was developed by Andreas Kadavanich using Crystal Maker.[39] It is interesting to note that in the image of the nanocrystal in the [100] orientation, Fig. 6A, the Cd and Se columns are nearly resolved. The spacing between the atomic columns in this orientation is 0.67 Å, just beyond the resolution of the microscope. The nanocrystal in Fig. 6B is in the [001] orientation, showing no mass contrast as the Se and Cd atomic columns are overlapped. Alternatively, the nanocrystal in Fig. 7A is in the [010] orientation where the Cd and Se atomic columns are separated, showing mass contrast. Also, a new orientation that had not been resolved prior to use of the aberration corrector is seen in Fig. 7B; it is the [111] orientation with a column separation of 2.75 Å.

Figs. 8A and B show two Z-STEM images of the TOPO/HDA nanocrystals with a zinc blende crystal structure. These nanocrystals do not exhibit the alternating ''zigzag'' pattern of a wurtzite nanocrystal. Also, these images exhibit a larger coating of the oxide layer, probably due to the light bulb treatment applied

Downloaded By: [Oak Ridge National Laboratory] At: 19:18 28 May 2009

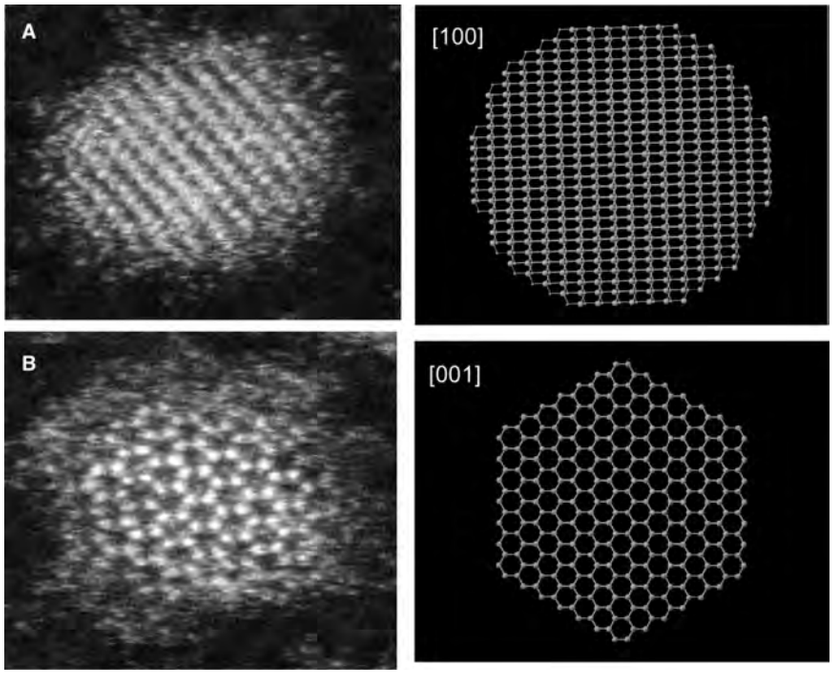

Fig. 6 Z-STEM images and model. The images obtained (A and B) can be directly compared to a traditional ball and stick model to determine orientation. The larger, orange atoms represent Cd while the smaller, blue atoms are Se. *Source*: Reprinted with permission from *Surf. Sci. Rep.*, **2007**, *62*, 111–157. © 2007 Elsevier B. V.

prior to imaging. Fig. 8A is a CdSe nanocrystal in the [010] orientation. This position shows the clearest mass contrast between the Cd and Se columns. However, a crystallographic defect can be seen in the image as there is an extra intensity source in between the atomic columns, probably indicating a stacking fault or twin boundary in the nanocrystal. The nanocrystal in Fig. 8B is also in the [010] orientation, but has a stacking fault parallel to the beam direction, indicated by the black line. In the case of the nanocrystal in Fig. 8B, two zinc blende phases are separated by a wurtzite stacking fault, forming a twin boundary. These low-energy defects in the crystal lattice are common for semiconducting nanocrystal systems.[40–42]

The nanocrystal in Fig. 8C shows the typical [001] pattern, but with faint ''spots'' situated directly in the center of the hexagons, as can be seen in the intensity profile (8F). The intensity profile shows that these peaks, marked by black arrows, are above the noise level in the image and appear perfectly spaced between the other atomic columns. This particular pattern is the result of a stacking fault midway through the nanocrystal that causes a shift of half of the crystal lattice. Figs. 8D and E show a model CdSe nanocrystal with a stacking fault that can reproduce the experimental image from the [001] and [010] orientations, respectively. The yellow arrow indicates the direction of the stacking fault.

The nanocrystal shown in Fig. 9A shows a relatively symmetrical intensity along its *C*-axis as would be expected for a traditional nanocrystal. The 3D cartoon (Fig. 9B) is helpful for visualizing the 3D shape of the nanocrystal. However, the nanocrystal in Fig. 9C clearly shows a large decrease in intensity for half of the nanocrystal, giving the impression that it is only partially completed or that a possible defect formation prevented further growth. An artist's conception of the approximate 3D shape is shown in Fig. 9D. From the 3D shape, it appears that the growth occurs in a stepwise manner, starting at a surface edge and then moving across while building upward along the *C*-axis. This most likely occurs due to the higher number of dangling bonds on the edges of the nanocrystal. With the surface clearly visible in these images, it should be feasible to observe subtle differences in surface structure caused by varying the surfactants, as illustrated in the following section.

SURFACTANT EFFECTS ON NANOCRYSTAL SURFACE STRUCTURE

It has been reported previously that CdSe nanocrystals prepared by the TOPO-only method are Cd rich.[43] It is believed that the excess Cd found in the TOPO-only nanocrystals resides in the elongated [101] facets, where there are two Se dangling bonds at each Se surface site. However, when an HDA was used as a co-surfactant, improvements in fluorescence quantum yield and narrower size distribution were also accompanied by a reduction in the excess cadmium measured. Z-STEM was used to image the CdSe

Downloaded By: [Oak Ridge National Laboratory] At: 19:18 28 May 2009

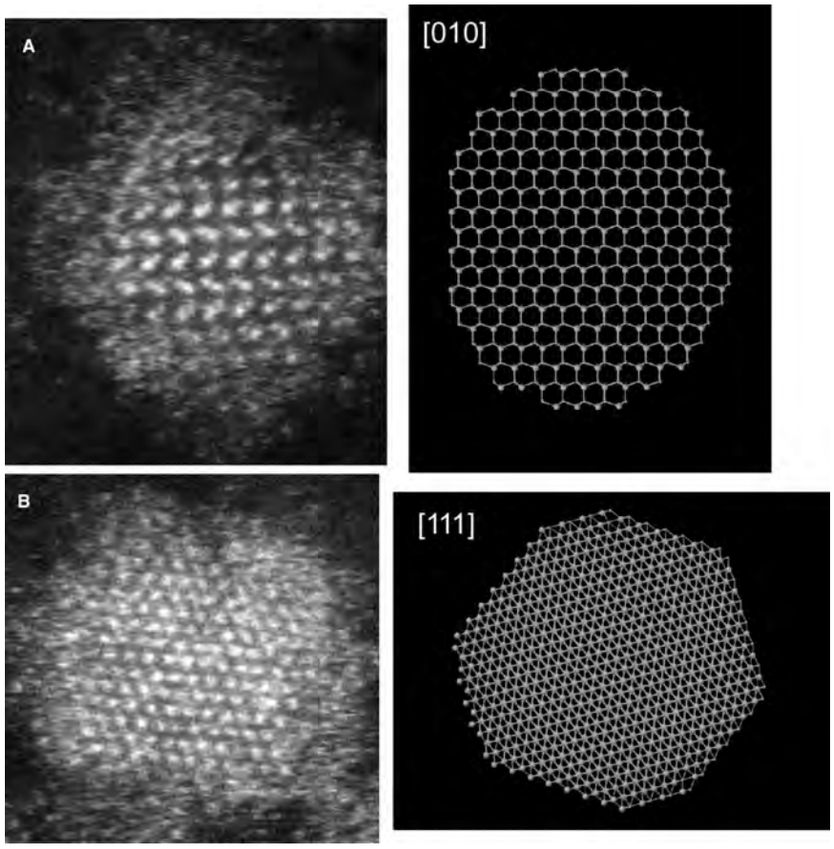

Fig. 7 Z-STEM images and model. (A) is a Z-STEM image of a CdSe nanocrystal showing atomic contrast with its associated model. (B) shows a peculiar spot patter that can be obtained by tilting a nanocrystal to the [111] orientation. *Source*: Reprinted with permission from *Surf. Sci. Rep.*, **2007**, *62*, 111–157. © 2007 Elsevier B. V.

nanocrystals produced under these two conditions and to determine any difference in surface structure.

The images in Fig. 10 are the first aberration-corrected Z-STEM images of CdSe nanocrystals ever taken, obtained shortly after the installation of the spherical aberration (C_s) corrector. The optimum probe size just after installation was around 0.8 Å, later demonstrated with the direct imaging of the 0.78 Å spacing in an Si [112] foil.[18] The striking detail of the surface of these nanocrystals prepared with TOPO as the only surfactant clearly shows the precise shape of the nanocrystals. Several of the nanocrystals in Fig. 10A appear elongated, while most exhibit an ovoid shape. The Z-STEM images clearly show a lack of shape distribution control. It was proposed that this might be the result of a ''magic'' impurity that exists in technical grade TOPO causing an increase in growth along the *C*-axis.[44] However, CdSe nanocrystals with a good size distribution cannot be grown without this ''magic'' impurity. Additionally, having too much of this impurity leads to uncontrolled growth. Prior to the Z-STEM reported here, it was determined by Peng and Peng that the magic ingredient was a phosphonic acid impurity in the TOPO that was necessary to control the shape and growth of the nanocrystals.[14] In addition to the phosphonic acid, a long-chain, primary amine, such as HDA, was also added to obtain superb size distribution without the need for size selective precipitation.[23] Atomic number contrast scanning transmission electron microscopy images of CdSe nanocrystals prepared with the mixture of TOPO/HDA and dodecylphosphonic acid, are shown in Fig. 10B. In both images, the large number of lattice-resolved nanocrystals illustrates the benefit of the Cs corrector and the small probe size. Since the nanocrystals are free to rotate, obtaining a good lattice-resolved image is dependent on the orientation of the nanocrystal during image capture. As the probe size decreases, the number of lattice-resolved nanocrystals increases due to improved ability to image nanocrystals off axis, and the higher number of zone-axis orientations that are resolvable. The small features seen near the surface would be very difficult to detect using conventional HRTEM.

Interestingly, a striking difference between the two images can be seen. Although the sizes of the nanocrystal samples differ only by 0.3 nm on average, their overall shape is markedly different. The TOPO-prepared CdSe nanocrystals in Fig. 10A appear to be elongated, compared with those of the TOPO/HDA-prepared nanocrystals in Fig. 10B. For example, the nanocrystal circled in Fig. 10C shows a definite

Downloaded By: [Oak Ridge National Laboratory] At: 19:18 28 May 2009

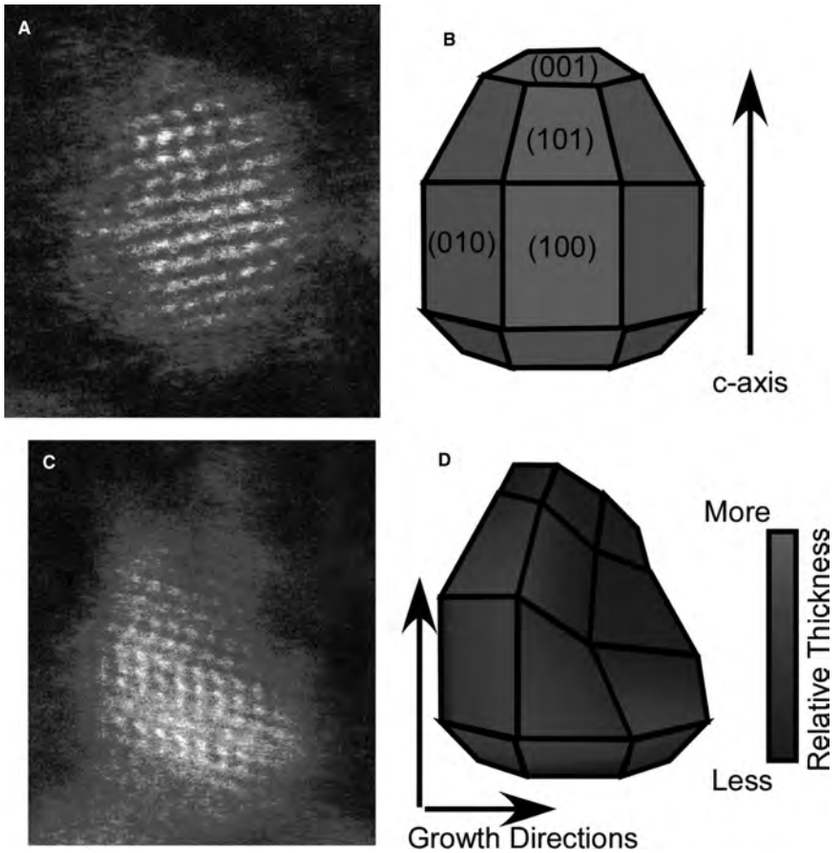

Fig. 8 (A) and (B) show Z-STEM images of CdSe nanocrystals with stacking faults perpendicular to the image plane. (C) is a Z-STEM image of a CdSe nanocrystal with a stacking fault in the image plane, adding intensity in the center of hexagons (D–F). *Source*: Reprinted with permission from *Surf. Sci. Rep.*, **2007**, *62*, 111-157. © 2007 Elsevier B. V.

narrowing along the *c*-axis, which is parallel to the surface plane. The inhomogeneous faceting of this sample is most likely the result of preferential growth along this axis. From this image, the orientation of the Cd and Se dumbbells can be determined, illustrated by the line profile in Fig. 10D, allowing us to assign the narrow end of the nanocrystal as the Se-rich (001′) face. This directly assigns the Se-rich face as the primary growth face and allows the direct determination of the remaining faces as shown in Fig. 10C. The growth direction and growth mode matches what was seen in more detail in the Z-STEM image of an ''incomplete'' nanocrystal in Fig. 9.

CHARACTERIZATION OF THE SHELL STRUCTURE OF CdSe-BASED CORE/SHELL NANOCRYSTALS

The ability of Z-STEM to simultaneously collect chemical information with structural position makes it an ideal tool for studying core/shell nanocrystals. The mass difference between the core and shell material manifests itself as a clear change in intensity in the raw images. Core-less, or ''dark,'' particles are easily identified in the same manner. We chose to study CdSe-based cores/shell systems since they have been previously characterized extensively. The purpose of the shell material is to passivate surface trap sites and to energetically confine the electron and hole. For high photoluminescence yields, ideally every absorbed photon will lead to the emission of a photon. To ensure radiative electron and hole recombination, a material with a wider band gap than the core is used to coat the surface. ZnS satisfies this requirement for CdSe cores, and is typically used as the shell material due. CdSe/ZnS is also an ideal test-bed for Z-STEM because of the large mass difference between the ZnS shell and the CdSe core. This work was performed in collaboration with Quantum Dot Corporation (now part of Invitrogen) to develop core/shell nanocrystals into commercially viable fluorescent probes.

Fig. 11A shows the first Z-STEM image of a CdSe/ZnS core/shell nanocrystal, prepared using the standard literature preparation by Quantum Dot Corp. with a core size of 3.0 nm and a measured fluorescence quantum yield of 34%.[11] The nanocrystal in the center of the raw Z-STEM image features a bright core, with a fainter shell encircling it. Lattice fringes seen on the shell indicate that it is crystalline; however,

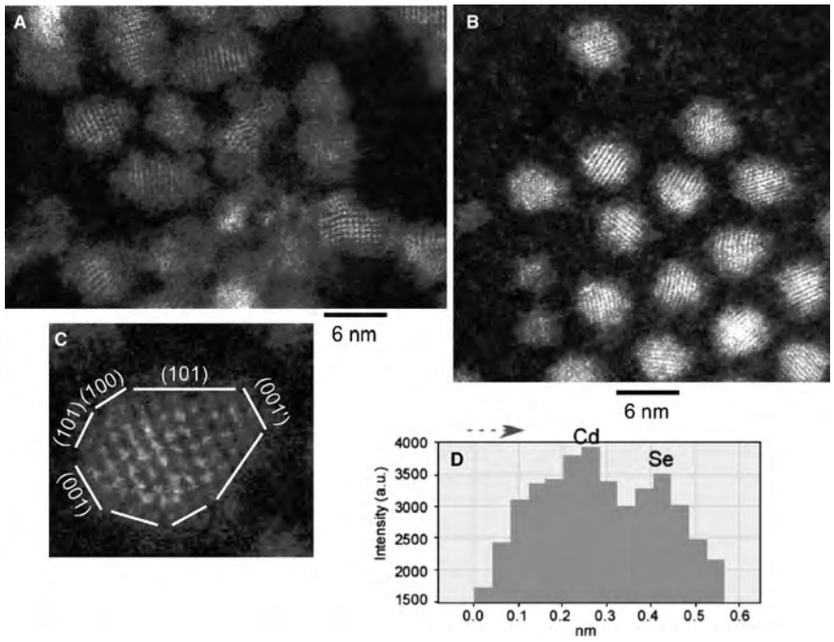

Fig. 9 Z-STEM and shape. The intensity contrast can be used to judge the overall nanocrystal shape. (A) is a regularly shaped nanocrystal with uniform intensity, illustrated by the cartoon (B). 7C shows a drastic decrease in intensity suggesting that the nanocrystal may not be complete, as illustrated by the cartoon (D). *Source*: Reprinted with permission from *Surf. Sci. Rep.*, **2007**, *62*, 111–157. © 2007 Elsevier B. V.

Downloaded By: [Oak Ridge National Laboratory] At: 19:18 28 May 2009

the shell is not spherical in shape and coats the core unevenly. From this image, the existence of core-less particles, presumably ZnS nanocrystals that nucleated during shell growth, are also seen. These dark particles can be clearly identified by their uniform intensity across the particle. Additionally, a large amount of excess starting material can be seen associated with the core/shell nanocrystals. This is surprising to find, given that the nanocrystals were washed several times. Finally, an amorphous or semicrystalline shell can be seen on the outermost surface of the core/shells, which is most likely an oxide coating on the ZnS shell.

Fig. 11B shows an extreme case where the ZnS shell only grew in one direction. This could be the result of the 11% lattice mismatch between CdSe and ZnS.[20] However, a more likely cause is the varied reactivity of the different nanocrystal surfaces. The Se rich, (001′) face of CdSe is unpassivated and typically the most reactive, and therefore it is the most likely place for shell growth to initiate. It is quite likely that this surface remains the most chemically reactive, since as the shell grows it remains the least passivated. This leads to a competitive growth process that often leaves the remainder of the core with little or no shell coverage, Fig. 11C shows a line profile along the *C*-axis of the core/shell in Fig. 11B, illustrating the intensity change going from shell to core due to the mass difference between the CdSe core and the ZnS shell. The interface between core and shell has been marked with a black arrow. The shell can be seen only covering one surface of the core. The large number of ZnS particles found is most likely due to the extreme excess of ZnS precursors that were used in an attempt to force the shell to grow on all the surfaces.

In general, the problem of growing a lattice-mismatched material onto a surface has been addressed before.[45–47] When a material is grown onto another material with different lattice spacing, strain energy is created as the chemical bonds are bent and stretched. For a cubic system, the strain energy areal density, E_ε, is given by Eq. (1).

$$E_\varepsilon = \varepsilon^2 B h \tag{1}$$

ε is defined as the in-plane strain, B is the bulk modulus for a thin film (for bulk CdSe, B is 5.5×10^{11} dyn/cm^2 at room temperature), and h is the film thickness. This thickness dependence leads to an important parameter called the critical thickness, h_c. In equilibrium, there is a maximum thickness of material that can be grown on a lattice-mismatched substrate before a dislocation forms. For growth on (100) cubic substrates, h_c is defined by Eq. (2).

$$h_c = \frac{b(1 - \nu\cos^2\Theta_{db})\left[\ln\left(\frac{h_c}{b}\right) + 1\right]}{8\pi(1 + \nu)f(\cos\lambda)} \tag{2}$$

In this equation, b is the Burgers vector, or the lattice constant of the defect, v is Poisson's ratio, f is the lattice mismatch, Θ is the angle between the dislocation and its Burgers vector, and λ is the angle between the slip direction, the direction that the defect propagates

Downloaded By: [Oak Ridge National Laboratory] At: 19:18 28 May 2009

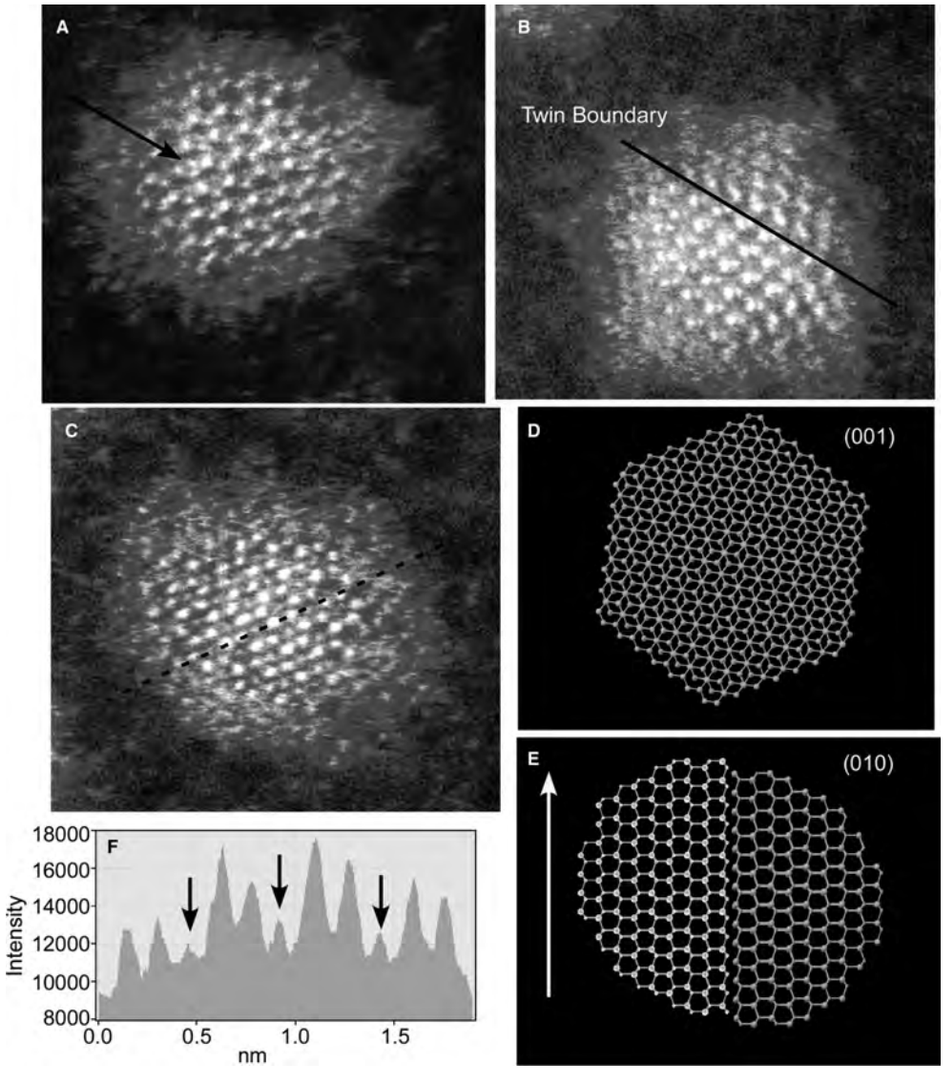

Fig. 10 TOPO vs. TOPO/HDA. (A) and (B) are Z-STEM images of CdSe nanocrystals prepared with TOPO and a mixture of TOPO and HDA, respectively. The TOPO only nanocrystals exhibit elongated facets (C). The relative intensity differences between atomic columns (D) seen in the images was used to identify the elongated facet as the (101) facet. *Source*: Reprinted with permission from *Nano Lett.*, **2004**, *4* (7) 1279–1283. © 2004 American Chemical Society.

and a line in the interface plane.[20] The important result of this relationship is that the critical thickness is inversely related to the lattice mismatch between the materials. Since the lattice mismatch between ZnS and CdSe is nearly 11%, h_c is less than 1 nm, so only a very thin ZnS shell can be grown before dislocations form. These dislocations could act as potential recombination centers, degrading the effectiveness of the shell. To obtain thicker shells, a shell material that has a smaller lattice mismatch with CdSe can be grown initially, followed by a thin coating of the material with a larger lattice mismatch. Two potential intermediate shell materials for the CdSe/ZnS core/shell system are CdS and ZnSe, which have lattice constants that reside between those of CdSe and ZnS.

Quantum Dot Corporation chose to introduce Cd in the shelling process to "dope" the shell to improve shell coverage. This method could produce either a $Zn_{(1-x)}Cd_xS$ shell or a CdSe/CdS/ZnS graded-shelled nanocrystal, Rutherford backscattering spectroscopy (RBS). RBS was used to confirm the addition of Cd to the shell, with an atomic ratio of Zn to Cd of 3 : 1, reduced from the 8 : 1 ratio found in the literature prepared sample.[44] This indicates that the majority of the shell contains Cd. Although the images (such as Fig. 11D) obtained do not clearly indicate an outer ZnS shell, owing to the varied reactivities of the cation precursors, it is quite likely that the majority of the zinc is coating the surface. Atomic number contrast scanning transmission electron microscopy images were

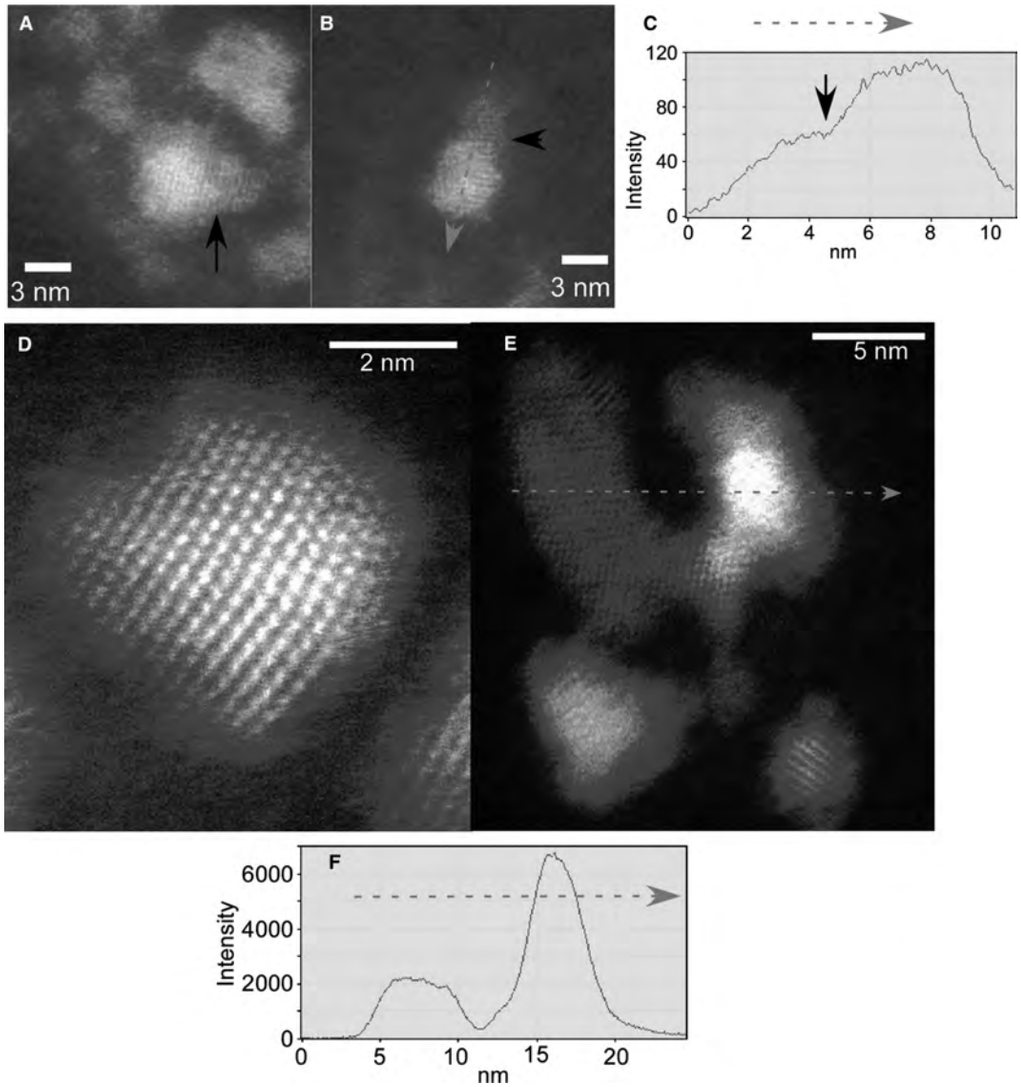

Fig. 11 Z-STEM of core/shell nanocrystals. (A) and (B) are images of CdSe/ZnS core/shell nanocrystals showing intensity contrast between core and shell (C). The black arrow in B and C indicates the interface between core and shell. (D) has cadmium doped into the shell, which improved shell coverage but reduced the amount of intensity contrast between core and shell. (E) shows a ZnS nanocrystal along side a core/shell nanocrystal with the associated intensity profile (F). Since the ZnS nanocrystal does not have a shell, the intensity remains uniform over its entirety. The dashed arrows indicate the position the where the intensity profiles (C and F) were obtained. Reprinted with permission from *Nano Lett.*, **2006**, *6* (7) 1496–1501. *Source*: © 2006 American Chemical Society.

obtained from the 3 nm core/shell/shell sample. This was the first core/shell/shell sample examined after the microscope was fitted with the C_s corrector. Fig. 11D shows the first lattice resolved image of a graded core/shell nanocrystal.

The square shape of the core/shell nanocrystal in 11D suggests that all sides are being coated. In comparison with the CdSe/ZnS quantum dot in Fig. 11B, the mass contrast between core and shell has diminished. This is most likely due to the structure being that of a core with a double shell of CdS/ZnS. The CdS acts as an intermediate layer, which improved total shell coverage when compared with that of a shell consisting of only ZnS. The increased ease of coating the quantum dot surface with CdS is manifested in the fact that the majority of the nanocrystals imaged in this sample are core/shells and not CdS or ZnS nanoparticles. Although the image in Fig. 11E was not typical of the sample, it does afford a unique opportunity to show the mass contrast difference between a core/shell nanocrystal and ZnS nanocrystal. This image features a core/shell nanocrystal associated with a long ZnS

Downloaded By: [Oak Ridge National Laboratory] At: 19:18 28 May 2009

Downloaded By: [Oak Ridge National Laboratory] At: 19:18 28 May 2009

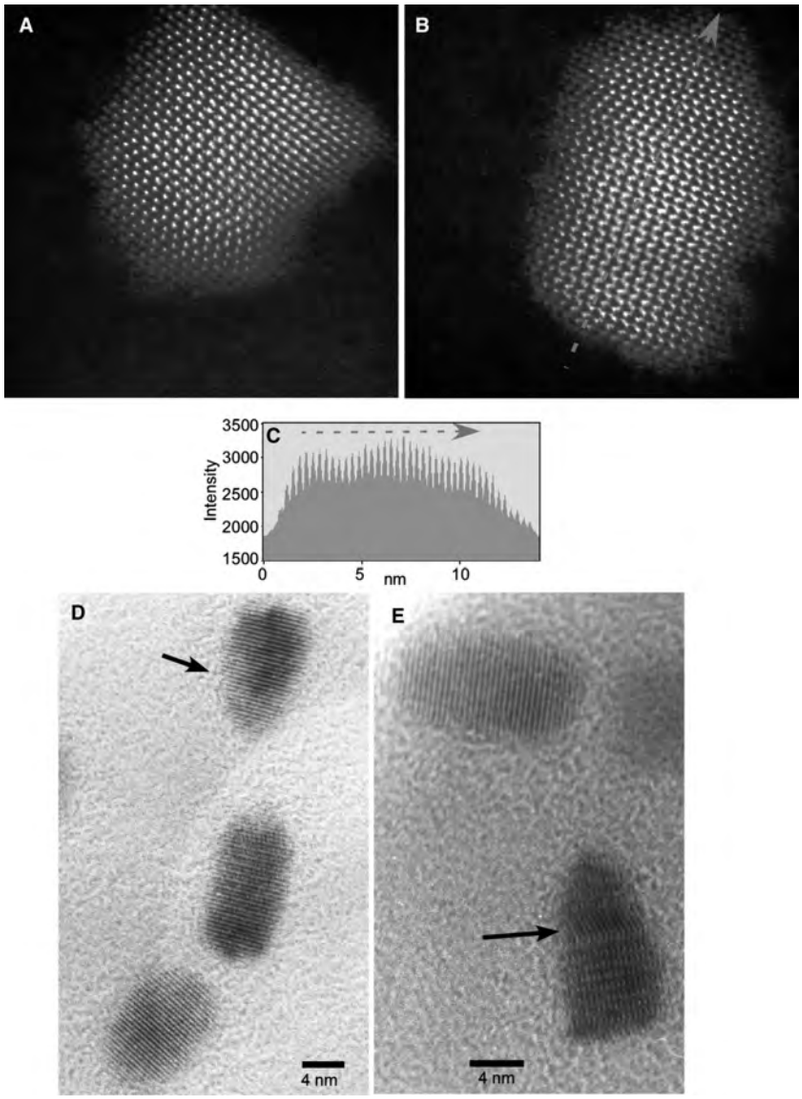

Fig. 12 Z-STEM of Qdot 655 core/shell nanocrystals. The core/shells (A and B) have a graded CdS/ZnS shell coating and exhibit a "nano-bullet" shape. Despite the graded shell, the overall coverage continues to prefer one particular surface over the others. 12C is the intensity profile taken along the c-axis showing a fairly uniform intensity profile until it begins to decrease near the tip. (D and E) are conventional TEM images of the same material with markers indicating contrast that can be misinterpreted as the result of the core/shell structure and is typical for nanocrystal rods. *Source*: Reprinted with permission from *Nano Lett.*, **2006**, *6* (7) 1496–1501. © 2006 American Chemical Society and from *Surf. Sci. Rep.*, **2007**, *62*, 111–157. © 2007 Elsevier B. V.

nanocrystal. The line profile, Fig. 11F, illustrates how easily ZnS particles can be identified by the image intensity. Since there is no change in the chemical composition, the ZnS particle has a nearly flat intensity profile, while the neighboring core/shell nanocrystal has a gaussian intensity profile. The intensity changes dramatically across the core/shell nanocrystal since the intensity is not only affected by the change in the amount of material but also by the change in chemical composition.

The double-shell method was also applied to the coating of CdSe nanorods with aspect ratios (length : width) near 2 : 1. The resulting core/shell/shell rods routinely have quantum efficiencies of 100% and are now commercially available from Invitrogen under the product names 655 and 605 AMP Quantum Dots. The initial number is the wavelength in nanometers of the emission maximum. These core/shells were coated with an AMP polymer that makes them water-soluble.[48] AMP stands for a generalized group of amphiphilic polymers, which have hydrophobic and hydrophilic end groups. The hydrophobic tails are used to interact with the hydrophobic surfactants on the surface of the nanocrystal. In the presence of water, the polymer forms a micelle around the quantum dot with the hydrophilic head groups forming the outer surface. These groups can then be cross-linked, essentially sealing the quantum dot in a "plastic bag."

The Z-STEM images in Fig. 12A and B show very little contrast between core and shell, since the shell is nearly all CdS. However, clear contrast can be seen between the intensities of the selenium and sulfur from the atomic dumbbells in the images. This is illustrated by the noticeable change in the appearance of the alternating dumbbells going from the center of the particle to the tip. The lesser intensity of the peaks in the atomic

dumbbell is from the anion, which in this case is the Se and S atomic columns. As the material transitions from predominantly CdSe/CdS to CdS, the anion intensity decreases to the point where only intensity from the Cd column can be seen. The abruptness of the loss of the anion intensity suggests that these particular nanorods may have a layered structure and are not an alloy.

Interestingly, the overall morphology deviates strongly from a homogeneous shell coating. The core/shell shape is that of a ''bullet,'' capped with a flat surface on one end while forming a point on the other. The line profile in Fig. 12C indicates very little intensity difference between core and shell. The sloping nature of the intensity profile near the tip of the nanorod is most likely due to a convolution of the lower atomic number of the shell material and the nanorod narrowing to a point. For comparison, Fig. 12D and E show two HRTEM images of the 655 AMP nanorods. The core/shell rod marked with an arrow in Fig. 12D appears to have some intensity contrast that could be attributed to the core/shell structure. However, none of the other rods in the same image show similar of contrast. This suggests that the contrast change is more likely a chromatic aberration effect, or the result of lattice strain, than actual contrast between different materials. Further evidence that the contrast change is not related to a core/shell structure is that similar contrast changes have been seen in nanorods that do not have a shell. The arrow in Fig. 12E points to a zinc blende stacking fault similar to the ones seen in the Z-STEM images (Fig. 12A and B).

Surprisingly, the Z-STEM images of the 605 AMP core/shell nanorods, Fig. 13A and B, appear narrower and more elongated in comparison with the 655 AMP ''nano-bullets.'' The shell covering the (001′) facet is nearly as thick as the core nanocrystal, as illustrated by the intensity profile in Fig. 13C. Additionally, this intensity profile shows a three-tiered structure that suggests three different chemical compositions. We can

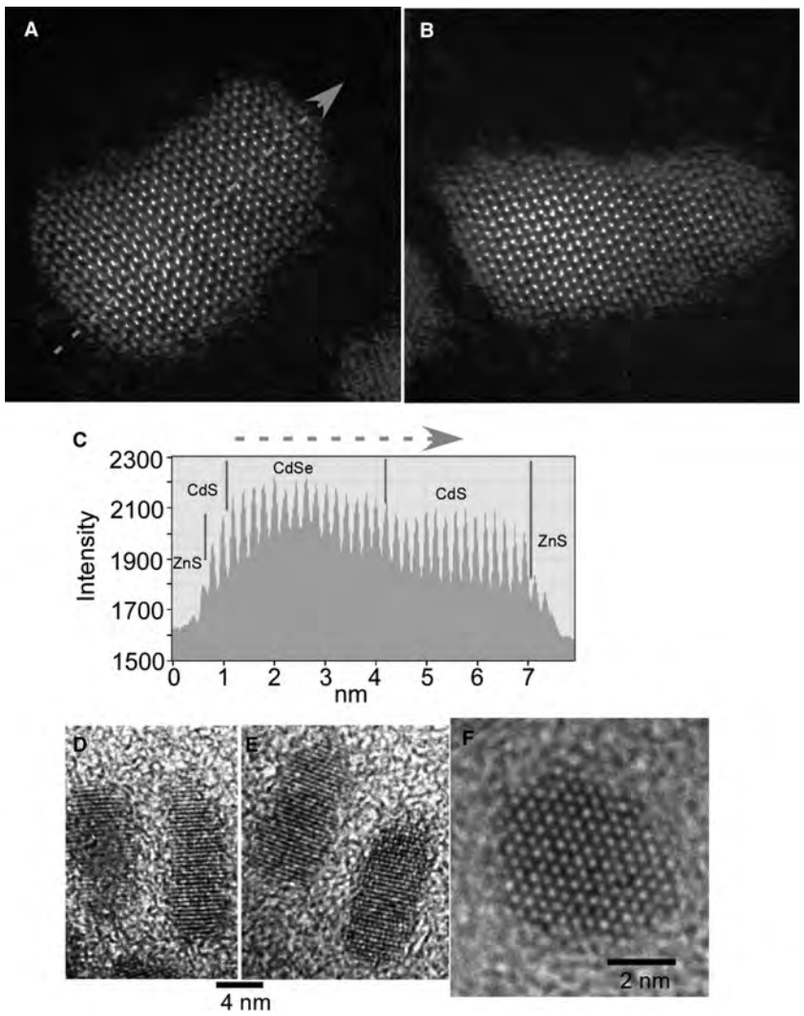

Fig. 13 Z-STEM of 605 Qdots. (A) and (B) are Z-STEM images of graded core/shell nanocrystals with the shell material predominantly coating one surface. The graded structure can be seen in the intensity profile (C). (D–F) are conventional TEM images of the same material, with F having the c axis perpendicular to the image plane. *Source*: Reprinted with permission from *Nano Lett.*, **2006**, *6* (7) 1496–1501. © 2006 American Chemical Society and from *Surf. Sci. Rep.*, **2007**, *62*, 111–157. © 2007 Elsevier B. V.

Downloaded By: [Oak Ridge National Laboratory] At: 19:18 28 May 2009

Downloaded By: [Oak Ridge National Laboratory] At: 19:18 28 May 2009

assign the highest-intensity region to the CdSe core, the intermediate region to the CdS inner shell and the edges to the ZnS outer shell. The other possibility is that the final two rows are also CdS but only covering a small portion of the surface. The filling of the {101} facets is not as evident in the majority of the 605 emitting core/shell rods; however, the shell material still covers the Se-rich faces preferentially. For comparison, Fig. 13D–F shows three HRTEM images of the 605 AMP core/shell nanorods. Fig. 13D and E are typical TEM images of this nanorod sample, showing a rounded end and a pointed end on each of the core/shell rods. Fig. 13F is a HRTEM image of a 605 AMP nanorod aligned with the (001) face perpendicular to the TEM grid. Although the surface is not well defined, the overall shape appears asymmetrical, which is most likely due to the shell coating certain surfaces preferentially. Unfortunately, no Z-STEM images of an on-end core/shell rod have been obtained owing to the extremely low occurrence of this orientation for rod-shaped nanocrystals.

Fig. 14 shows Z-STEM images of the 605 AMP core/shell rods whose shell surfaces are clearly resolved. Several gaps and outgrowths, marked with a white oval can be seen, showing that the shell is not perfect at its surface. If tunneling of charges through the shell occurs, these defects would serve as potential trap sites due to the presence of unsatisfied bonds. However, this sample has a quantum yield of nearly 100%, indicating that the ability of an electron or hole to tunnel to the shell surface is limited. This means that the shell surface need not be perfect, but instead that the shell only needs to cover the entire surface of the core, to effectively passivate the core.

The level of atomic detail afforded by Z-STEM can be used to identify specific nanocrystal faces of core/shell nanocrystals. This is important because the CdSe nanocrystal facets are not chemically equivalent, which may explain why the coating of the shell is not uniform. As illustrated by the cartoon in Fig. 15, once the alternating intensity pattern of the Cd and Se dumbbells is identified (Fig. 15B), we can then assign one end of the rod as the Se-rich (001′) face and the other as the Cd-rich (001) face. A comparison of the image to a model of the CdSe core (Fig. 15C) can then be used to identify the remaining surfaces. The image in Fig. 15D exhibits the typical "nano-bullet" shape, with a near perfectly flat end opposite a pointed end. Using the atomic dumbbells, we can definitively assign the pointed end of the nanorod as the anion rich (001′) face. This supports predictions in the literature stating that the Se-rich face is the primary growth face for the CdSe core.[23] The facets with the next highest concentration of Se surface sites are the (101′) facets, located near the flat end of the "nano-bullet" (marked with a blue arrow). Interestingly, to achieve the unique bullet shape, these corner (101′) facets must also grow at a faster rate than the side (100) faces. The shell appears to be at its thinnest on the Cd-rich (001) and the {100} surfaces, with an average coverage of a

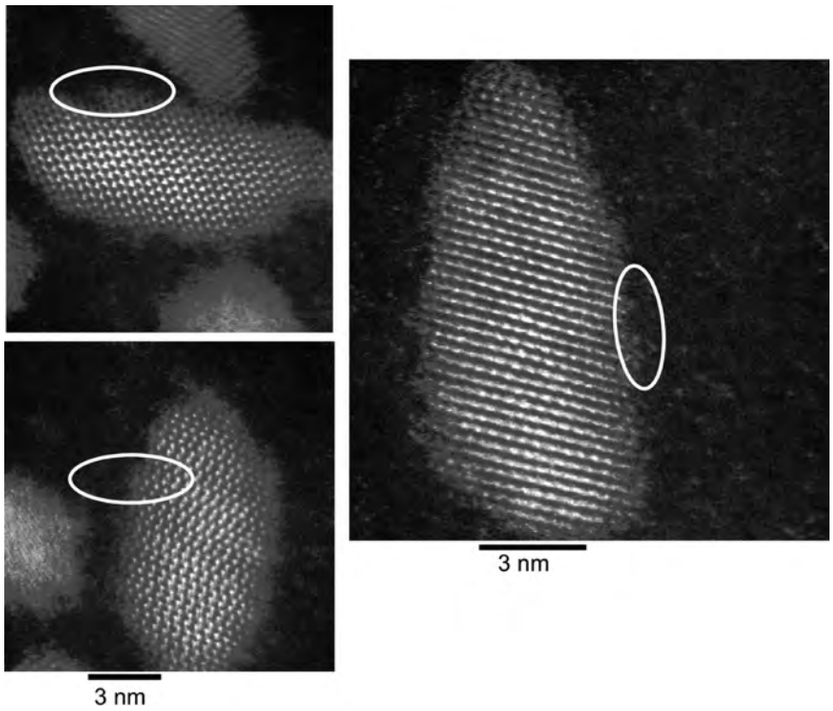

Fig. 14 Z-STEM images of core/shell surface. Defects such as missing atomic columns can be seen on the shell surface (circled). *Source*: Reprinted with permission from *Surf. Sci. Rep.*, **2007**, *62*, 111–157. © 2007 Elsevier B. V.

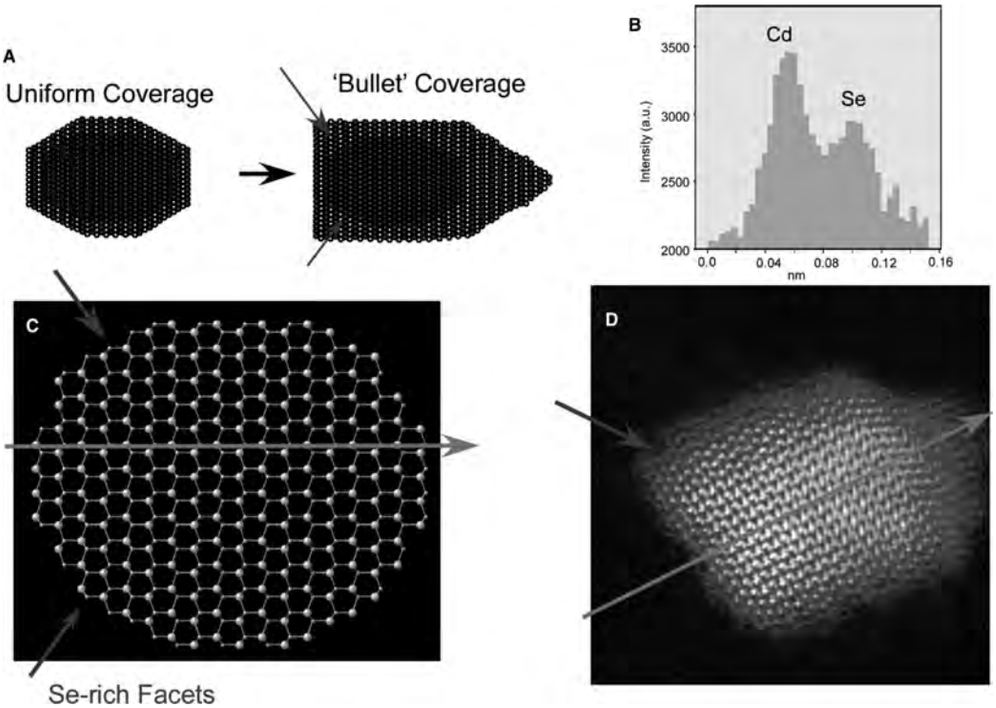

Fig. 15 Shell Growth Model. (A) shows a cartoon illustration of the difference between the predicted core/shell structure and the obtained "nano-bullet" shape. From atomic dumbbell contrast (B) one can orientate a model (C) to an image of a core/shell nanocrystal (D). With this simple comparison, it would appear that the shell is preferentially growing on the anion rich surfaces. *Source*: Reprinted with permission from *Nano Lett.*, **2006**, *6* (7) 1496–1501. © 2006 American Chemical Society.

monolayer or two, while the Se-rich {101′} facets have about 4–5 monolayers and the (001′) facet has anywhere from 6 to 15 monolayers. Thus, the shell-growth mechanism appears to select the anion surface sites preferentially.

Fig. 16 shows a CdSe/CdS core/shell nanorod oriented with the (010) face parallel to the TEM grid. The atomic dumbbells are clearly resolved in the raw image and can easily be assigned by their mass contrast. In Fig. 16B, a Fourier filter has been used to reduce the amount of noise in the image to better show the mass contrast. This rod was resting on an edge, as illustrated by the model in Fig. 16D and provides a unique opportunity to illustrate how structure in the *z*-direction (out of the image plane) can be obtained from the raw image. The intensity profile in Fig. 16C beautifully outlines the faceted shape of the nanocrystal surface that coincides with this orientation. Lastly, the intensity profile in Fig. 16E shows how cleanly the individual atomic columns are resolved in the image. In this single image, we can see the atomic structure, identify specific facets, and determine the core/shell rod's 3D shape.

The Z-STEM images and the near unity quantum yield of the AMP-coated core/shell nanorods suggest that shell coverage free of interfacial defects is more important than electron and hole confinement. Presumably, in the case of ZnS, defects in the shell or a lack of complete shell coverage provide tunneling sites or surface sites for non-radiative recombination. This is supported by the result that the largest improvement in fluorescence quantum yield was realized by choosing a better lattice-matched material at the expense of electron confinement. Elimination of dark particles is also important, resulting in another 20% increase in fluorescence quantum yield. However, the role of Zn in the core/shell/shell system remains important. Core/shell rods made with only a CdS shell were found to be far less photostable than those containing Zn. The role of ZnS as a photostabilizing layer has been supported by previous work, in which CdSe cores with ZnS shells demonstrated an improved photostability over cores with a CdS shell.[22] This is most likely due to the CdS shell absorbing at 366 nm, which is the wavelength commonly used for fluorescence imaging. Since bulk ZnS absorbs at 345 nm and below, a ZnS shell should only absorb at even lower wavelengths (due to quantum confinement), making it less susceptible to photodegradation under typical experimental conditions. In this system, the benefit of a lattice-matched CdS shell has been combined with the photostability of the ZnS shell to make very bright and stable core/shell nanocrystals.

Downloaded By: [Oak Ridge National Laboratory] At: 19:18 28 May 2009

Downloaded By: [Oak Ridge National Laboratory] At: 19:18 28 May 2009

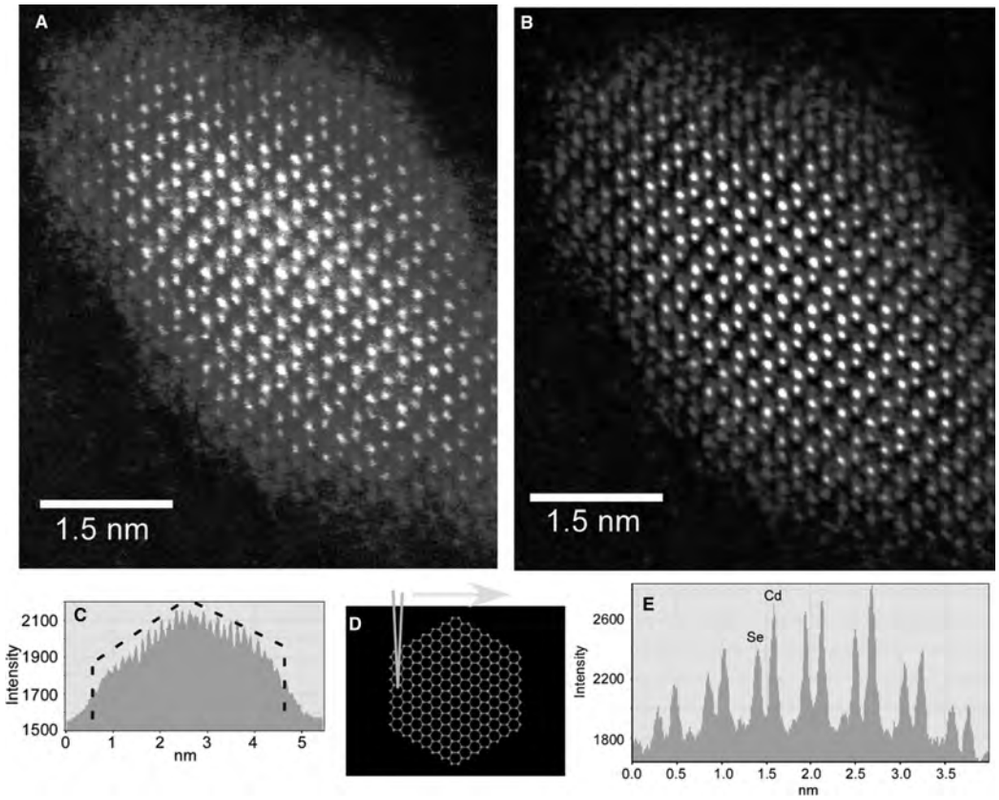

Fig. 16 Nanocrystal Hand-stand. (A) (raw) and (B) (Fourier filtered) are Z-STEM images of a core/shell rod in the (010) orientation. The intensity profile (C) shows the shape of the nanocrystal with a facet rising out of the image plane. (D) illustrates the nanocrystal orientation relative to the electron beam (green) and scan direction (green arrow). (E) is an intensity profile from B showing atomic contrast and thickness contrast simultaneously. *Source*: Reprinted with permission from *Nano Lett.*, **2006**, *6* (7) 1496–1501. © 2006 American Chemical Society.

Z-STEM OF $CdSe_xS_{(1-x)}$ ALLOYS

$CdSe_xS_{(1-x)}$ alloys have the potential for use as fluorescent probes when multiple emission colors are needed without resorting to changing the diameter of the nanocrystals. For example, work by Bawendi et al. illustrates the need to consider the effects of the nanocrystal's hydrodynamic radius when conducting a fluorescence imaging experiment in vivo.[49] By changing the relative amounts of the two anions, the band gap can be adjusted while maintaining the nanocrystal diameter.

Alloy nanocrystals were synthesized by using the method of Swafford, where the composition was controlled by adjusting the relative amounts of the anions found in the injection solution.[17] The composition of the nanocrystal was determined by RBS analysis on purified aliquots pulled during growth. However, although the RBS data suggests that the relative amounts of sulfur and selenium remained constant during growth, sequestering of one the anions or the nucleation of non-alloyed nanocrystals could not be ruled out from the RBS analysis alone. Z-STEM was employed to demonstrate uniform distribution of the anions throughout the nanocrystals. If the nanocrystals exhibited a core/shell structure in the Z-STEM images, this would indicate that the elements were sequestering during growth.

Fig. 17A and B show the Z-STEM images of $CdS_{0.55}Se_{0.45}$. Unlike the core/shell images shown earlier, there is no noticeable change in intensity across the nanocrystal. However, the nanocrystals exhibit a zinc blende structure with a large number of stacking faults that can be seen on nearly every nanocrystal. To determine whether this was a result of the alloying process or an affect of the oleic acid surfactant, CdSe nanocrystals prepared using oleic acid as the surfactant were also imaged. Fig. 17C shows Z-STEM images of CdSe prepared in oleic acid. The CdSe nanocrystals are also zinc blende, unlike those produced in TOPO and appear to have the same large number of stacking faults as seen for the alloys. This suggests that the zinc blende structure and number of stacking faults is the result of the surfactant and not the alloying process.

Downloaded By: [Oak Ridge National Laboratory] At: 19:18 28 May 2009

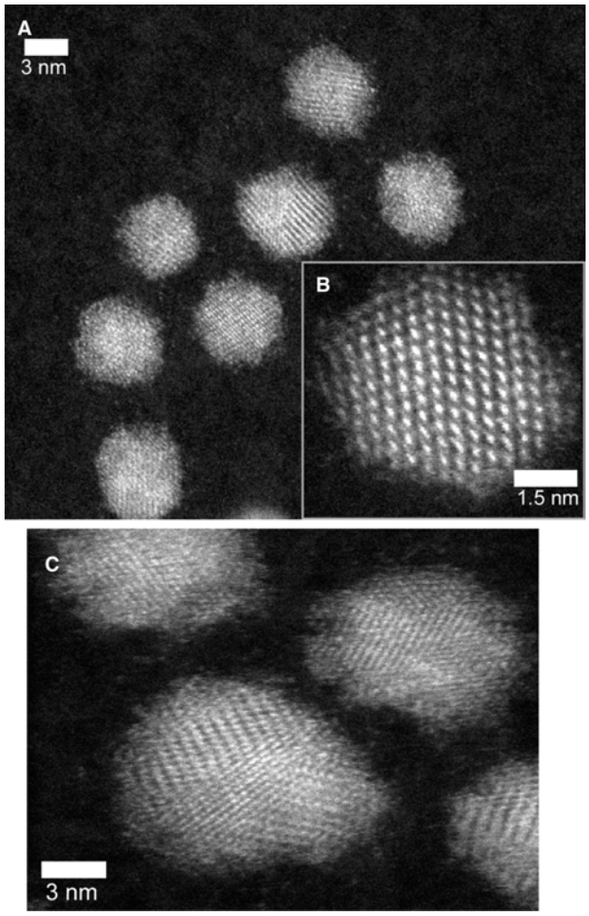

Fig. 17 Z-STEM of CdS0.55Se0.45 alloyed nanocrystal. (A) and (B) are Z-STEM images of alloyed nanocrystals showing large number of stacking fault but no contrast due to sequestering or core/shell structures. (C) is an image of CdSe nanocrystals prepared using oleic acid. In contrast to nanocrystals synthesized in TOPO/HDA, there are a large number of stacking faults and twinning, the result of the oleic acid surfactant.

CONCLUSION

The use of aberration-corrected Z-STEM has provided a clearer understanding of the surface structure of nanocrystals and its importance in growth. For the first time, it was possible to image, with atomic-scale precision, the surface of a nanocrystal. The result of this has allowed for the accurate assignment of the nanocrystal surfaces and uses that to formulate a mechanism for nanocrystal growth and, in a similar fashion, shell growth.

From the Z-STEM images obtained and the chemistry employed, our current understanding of nanocrystal growth involves a dynamic competition between the different reactivities of the nanocrystal surface. Growth is predominantly along the *C*-axis from the anion terminated surface, with a rate dependent on the amount of phosphonic acid and aliphatic amine used in the reaction. The growth of a symmetrical epitaxial shell is also hindered by the highly reactive anion-rich facets leading to certain surfaces with very little shell and others with a large excess. Homogeneous nanocrystal alloys are possible; however, the use of oleic acid produces nanocrystals with large numbers of stacking faults.

ACKNOWLEDGEMENTS

This research was sponsored by the Office of Basic Energy Sciences, Division of Materials Sciences and Engineering, DOE grant FG02-02ER45957 and NIH RO1 EB003728-02.

REFERENCES

1. Brus, L.E. Electron-electron and electron-hole interaction in small semiconductor crystallites: the size dependence of the lowest excited electronic state. J. Chem. Phys. **1984**, *80* (9), 4403–4408.
2. Murray, C.B.; Norris, D.J.; Bawendi, M.G. Synthesis and characterization of nearly monodisperse CdE (E = S, Se, Te) semiconductor nanocrystallites. J. Am. Chem. Soc. **1993**, *115*, 8706–8715.
3. Bruchez, M.; Moronne, M.; Gin, P.; Weiss, S.; Alivisatos, A.P. Semiconductor nanocrystals as fluorescent biological labels. Sci. Rep. **1998**, *281*, 2013–2015.
4. Colvin, V.L.; Schlamp, M.C.; Alivisatos, A.P. Light-emitting diodes made from cadmium selenide nanocrystals and a semiconducting polymer. Nature **1994**, *370* (4), 354–357.
5. Gao, X.; Cui, Y.; Levenson, R.M.; Chung, L.W.K.; Nie, S. In vivo cancer targeting and imaging with semiconductor quantum dots. Nat. Biotechnol. **2004**, *22* (8), 969–976.
6. Gao, X.; Yang, L.; Petros, J.A.; Marshall, F.F.; Simons, J.W.; Nie, S. In vivo molecular and cellular imaging with quantum dots. Curr. Opin. Biotechnol. **2005**, *16*, 63–72.
7. Goldman, E.R.; Clapp, A.R.; Anderson, G.P.; Uyeda, H.T.; Mauro, J.M.; Medintz, I.L.; Mattoussi, H. Multiplexed toxin analysis using four colors of quantum dot fluororeagents. Anal. Chem. **2004**, *76* (3), 684–688.
8. Huynh, W.U.; Dittmer, J.J.; Alivisatos, A.P. Hybrid nanorod-polymer solar cell. Science **2002**, *295*, 2425–2427.
9. Rosenthal, S.J.; Tomlinson, I.; Adkins, E.M.; Schroeter, S.; Adams, S.; Swafford, L.; McBride, J.; Wang, Y.; DeFelice, L.J.; Blakely, R.D. Targeting cell surface receptors with ligand-conjugated nanocrystals. J. Am. Chem. Soc. **2002**, *124*, 4586–4594.
10. Schlamp, M.C.; Peng, X.; Alivisatos, A.P. Improved efficiencies in light emitting diodes made with CdSe(CdS) core/shell type nanocrystals and a semiconducting polymer. J. Appl. Phys. **1997**, *82* (11), 5837–5842.

Downloaded By: [Oak Ridge National Laboratory] At: 19:18 28 May 2009

11. Manna, L.; Scher, E.; Li, L.; Alivisatos, A.P. Epitaxial growth and photochemical annealing of graded CdS/ZnS shells on colloidal CdSe nanorods. J. Am. Chem. Soc. **2002**, *124* (24), 7136–7145.
12. Bowen-Katari, J.E.; Colvin, V.L.; Alivisatos, A.P. X-ray photoelectron spectroscopy of CdSe nanocrystals with applications to studies of the nanocrystal surface. J. Phys. Chem. **1994**, *98*, 4109–4117.
13. Peng, Z.A.; Peng, X. Formation of high-quality CdTe, CdSe, and CdS nanocrystals using CdO as precursor. J. Am. Chem. Soc. **2001**, *123*, 183–184.
14. Peng, Z.A.; Peng, X. Mechanisms of the shape evolution of CdSe nanocrystals. J. Am. Chem. Soc. **2001**, *123*, 1389–1395.
15. Qu, L.; Peng, A.Z.; Peng, X. Alternative routes toward high quality CdSe nanocrystals. Nano Lett. **2001**, *1* (6), 333–337.
16. Yu, W.W.; Peng, X. Formation of high-quality CdS and other II-VI semiconductor nanocrystals in noncoordinating solvents: tunable reactivity of monomers. Angew. Chem. Int. Ed. **2002**, *41* (13), 2368–2371.
17. Swafford, L. Homogeneously alloyed cadmium sulfoselenide nanocrystals. In *Chemistry*; Vanderbilt University: Nashville, 2006.
18. Nellist, P.D.; Chisholm, M.F.; Dellby, N.; Krivanek, O.L.; Murfitt, M.F.; Szilagyi, Z.S.; Lupini, A.R.; Borisevich, A.; Sides, W.H., Jr.; Pennycook, S.J. Direct sub-angstrom imaging of a crystal lattice. Science **2004**, *305*, 1741.
19. Shiang, J.J.; Kadavanich, A.V.; Grubbs, R.K.; Alivisatos, A.P. Symmetry of annealed wurtzite CdSe nanocrystals: Assignment to the C_{3v} point group. J. Phys. Chem. **1995**, *99*, 17,417–17,422.
20. Tu, K.; Mayer, J.W.; Feldman, L.C. *Electronic Thin Film Science*; Macmillan Publishing Company: New York City, 1992.
21. Peng, X.; Manna, L.; Yang, W.; Wickham, J.; Scher, E.; Kadavanich, A.; Alivisatos, A.P. Shape control of CdSe nanocrystals. Nature **2000**, *404* (2), 59–61.
22. Mekis, I.; Talapin, D.V.; Kornowski, A.; Haase, M.; Weller, H. One-pot synthesis of highly luminescent CdSe/CdS core-shell nanocrystals via organometallic and ''greener'' chemical approaches. J. Phys. Chem. B **2003**, *2003* (107), 7454–7462.
23. Talapin, D.V.; Koeppe, R.; Gotzinger, S.; Kornowksi, A.; Lupton, J.M.; Rogach, A.L.; Benson, O.; Feldmann, J.; Weller, H. Highly emissive colloidal CdSe/CdS heterostructures of mixed dimensionality. Nano Lett. **2003**, *3* (12), 1677–1681.
24. Krivanek, O.L.; Nellist, P.D.; Dellby, N.; Murfitt, M.F.; Szilagyi, Z. Towards sub-0.5 angstrom electron beams. Ultramicroscopy **2003**, *96*, 229–237.
25. Kadavanich, A.V.; Kippeny, T.C.; Erwin, M.M.; Pennycook, S.J.; Rosenthal, S.J. Sublattice resolution structural and chemical analysis of individual CdSe nanocrystals using atomic number contrast scanning transmission electron microscopy. J. Phys. Chem. B **2001**, *105* (2), 361–369.
26. Nellist, P.D.; Pennycook, S.J. Incoherent imaging using dynamically scattered coherent electrons. Ultramicroscopy **1999**, *78* (1–4), 111–124.
27. Pennycook, S.J.; Nellist, P.D. Z-contrast scanning transmission electron microscopy. In *Impact of Electron Scanning Probe Microscopy on Materials Research*; Rickerby, D., Valdre, G., Valdre, U., Eds.; Kluwer Academic Publishers: The Netherlands, 1999.
28. Borisevich, A.Y.; Lupini, A.R.; Travaglini, S.; Pennycook, S.J. Depth sectioning of aligned crystals with the aberration-corrected scanning transmission electron microscope. J. Elect. Micros. **2006**, *55* (1), 7–12.
29. Varela, M.; Findlay, S.D.; Lupini, A.R.; Christen, H.M.; Borisevich, A.Y.; Dellby, N.; Krivanek, O.L.; Nellist, P.D.; Oxley, M.P.; Allen, L.J.; Pennycook, S.J. Spectroscopic imaging of single atoms within a bulk solid. Phys. Rev. Lett. **2004**, *92* (9), 095502.
30. Arslan, I.; Yates, T.J.V.; Browning, N.D.; Midgley, P.A. Embedded nanostructures revealed in three dimensions. Science **2005**, *309*, 2195–2198.
31. Yan, Y.; Chisholm, M.F.; Duscher, G.; Maiti, A.; Pennycook, S.J.; Pantelides, S.T. Impurity-induced structural transformation of a MgO grain boundary. Phys. Rev. Lett. **1998**, *81* (17), 3675–3678.
32. Chisholm, M.F.; Maiti, A.; Pennycook, S.J.; Pantelides, S.T. Atomic configurations and energetics of arsenic impurities in a silicon grain boundary. Phys. Rev. Lett. **1998**, *81* (1), 132135.
33. McGibbon, M.M.; Browning, N.D.; Chisholm, M.F.; McGibbon, A.J.; Pennycook, S.J.; Ravikumar, V.; Dravid, V.P. Direct determination of grain boundary atomic structure in $SrTiO_3$. Science **1994**, *266*, 102–104.
34. Browning, N.D.; Chisholm, M.F.; Pennycook, S.J.; Norton, D.P.; Lowndes, D.H. Correlation between hole depletion and atomic structure at high-angle grain boundaries in $YBa_2Cu_3O_{7-d}$. Physica C **1993**, *212* (1–2), 185–190.
35. Varela, M.; Lupini, A.R.; Benthem, K.V.; Borisevich, A.Y.; Chisholm, M.F.; Shibata, N.; Abe, E.; Pennycook, S.J. Materials characterization in the aberration-corrected scanning transmission electron microscope. Ann. Rev. Mater. Res. **2005**, 539–569.
36. Shibata, N.; Pennycook, S.J.; Gosnell, T.R.; Painter, G.S.; Shelton, W.A.; Becher, P.F. Observation of rare-earth segregation in silicon nitride ceramics at subnanometer dimensions. Nature **2004**, *428*, 730–733.
37. Borisevich, A.Y.; Lupini, A.R.; Pennycook, S.J. Depth sectioning with the aberration-corrected scanning transmission electron microscope. Proc. Natl Acad. Soc. **2006**, *103* (9), 3044–3048.
38. Rosenthal, S.J.; McBride, J.; Pennycook, S.J.; Feldman, L.C. Synthesis, surface studies, composition and structural characterization of CdSe, core/shell and biologically active nanocrystals. Surf. Sci. Rep. **2007**, *62*, 111–157.
39. Palmer, D. *Crystal Maker*; Crystal Maker Software, 1994.
40. Manna, L.; Scher, E.C.; Alivisatos, A.P. Synthesis of soluble and processable rod-, arrow-, teardrop-, and tetrapod-shaped CdSe nanocrystals. J. Am. Chem. Soc. **2000**, *122*, 12,700–12,706.
41. Rogach, A.L.; Kornowski, A.; Gao, M.; Eychmuller, A.; Weller, H. Synthesis and characterization of a size series of extremely small thiol-stabilized CdSe. J. Phys. Chem. B **1999**, *103*, 3065–3069.

42. Wei, S.; Zhang, S.B. Structure stability and carrier localization in CdX (X = S, Se, Te) semiconductors. Phys. Rev. B **2000**, *62* (11), 6944–6946.
43. Taylor, J.; Kippeny, T.; Rosenthal, S.J. Surface stoichiometry of CdSe nanocrystals determined by Rutherford backscattering spectroscopy. J. Clust. Sci. **2001**, *12* (4), 571–582.
44. McBride, J.; Treadway, J.; Feldman, L.C.; Pennycook, S.J.; Rosenthal, S.J. Structural basis for near unity quantum yield core/shell nanocrystals. Nano Lett. **2006**, *6* (7), 1496–1501.
45. Amano, H.; Sawaki, N.; Akasaki, I. Metalorganic vapor phase eptiaxial growth of a high quality GaN film using an AlN buffer layer. Appl. Phys. Lett. **1985**, *48* (5), 353–355.
46. Lincot, D.; Kampmann, A.; Mokili, B.; Vedel, J. Epitaxial electrodeposition of CdTe films on InP from aqueous solutions: role of a chemically deposited CdS intermediate layer. Appl. Phys. Lett. **1995**, *67* (16), 2355–2357.
47. Wu, X.; Peng, Z.; Yuan, S. Interface structure of CdSe/ZnSe epilayers. J. Appl. Phys. **1995**, *77* (8), 3818–3822.
48. Pellegrino, T.; Manna, L.; Kudera, S.; Liedl, T.; Koktysh, D.; Rogach, A.L.; Keller, S.; Radler, J.; Natile, G.; Parak, W.J. Hydrophobic nanocrystals coated with an amphiphilic polymer shell: a general route to water soluble nanocrystals. Nano Lett. **2004**, *4* (4), 703–707.
49. Zimmer, J.P.; Kim, S.; Ohnishi, S.; Tanaka, E.; Frangioni, J.V.; Bawendi, M.G. Size series of small indium arsenide-zinc selenide core-shell nanocrystals and their application to in vivo imaging. J. Am. Chem. Soc. **2006**, *128*, 2526–2527.

Downloaded By: [Oak Ridge National Laboratory] At: 19:18 28 May 2009